SEECCM III
3rd South-East European Conference on Computational Mechanics-
an ECCOMAS and IACM Special Interest Conference
M. Papadrakakis, M. Kojic, I. Tuncer (eds.)
Kos Island, Greece, 12–14 June 2013

Study of Asymmetric Glass Reinforced Plastic Beams in Off-Axis Four-Point Bending

Efstathios E. Theotokoglou[1] **and Emilio P. Sideridis**[1]

[1] School of Applied Mathematical and Physical Sciences,
Department of Mechanics Laboratory of Testing and Materials,
The National Technical University of Athens, Zographou Campus,
Theocaris Bld., GR-0157 73, Athens, Greece
stathis@central.ntua.gr

Keywords: Asymmetric Glass Reinforced Plastic Beams, Off-Axis Four Point Bending, Computational Analysis, Stress Analysis, Composite Materials, Interlaminar Shear Strength.

Abstract. *The present paper deals with the computational study of asymmetric glass reinforced plastic beams in off-axis four point bending and the comparison of the induced results with experimental and analytical results. The measurement of the interlaminar shear strength of composite beams, an important design variable in many applications, may be successfully performed by the asymmetric bending test. A three dimensional finite element analysis is adopted throughout the composite beams in order to, on the one hand, correlate with the experimental results and, on the other hand to obtain the stress distributions at the supports and at the loading points where usually there is an abrupt variation due to the indentation existing because of the noses. From the Finite Element Analysis and the experimental investigation possible crack initiation positions are determined.*

.

1 INTRODUCTION

The glass reinforced plastic (GRP), pipes and components are widely used in the process plant and chemical industries in applications requiring corrosion resistance. Also the need to reduce vehicle weight and consideration for mass production techniques, among other things, has led the automotive industry to consider randomly-oriented chopped-fibre reinforced plastics as near-term substitutes for steel in structural panels.

In order to perform stress and stiffness analyses of chopped-fibre/resin composites, it is essential that the properties be known since in general these materials appear as anisotropic and heterogeneous. But if the fibres are randomly distributed with respect to orientation and position then samples of material which contain statistically significant numbers of fibres will appear to be isotropic. If several such samples are compared, the composite will appear to be homogeneous. If the fibres have a preferred orientation, then the composite will appear to be anisotropic.

Since, the composite panel properties depend on the elastic properties and volume fractions of the constituent materials and are affected by the fabrication techniques and most of them are stiffness or strength designed it is useful to investigate this subject.

An important property which affects the application of glass-reinforced plastics (GRP) is the interlaminar shear strength, which characterizes the interface between fibre and matrix [1]. As a result of low interlaminar shear strength, failure of the composite often occurs in the interlaminar region. Possible interlaminar shear failures have been observed due to high transverse shear forces arising as a result of large changes in bending moment along or around a beam or a shell under combined loading. Such conditions can occur in a pipe where the thickness changes, are abrupt and excessive, and can be produced with internal pressure [2] (or other types of loading [3]), or in smooth pipe bends under flexure [4, 5]. Consequently the interlaminar shear strength is an important design parameter in many applications. Since there is a need for reliable data, a testing procedure for determining interlaminar shear properties has already been developed [6]. The interlaminar fracture toughness in end notched flexure specimens [7] and the interlaminar shear fracture of interleaved graphite/epoxy composites [8] have been examined. The fracture of sandwich beams in three point bending has also been considered [9, 10].

Material	E_x (GPa)	E_y (GPa)	E_z (GPa)	ν_{xy}	ν_{xz}	ν_{yz}	G_{xy} (GPa)	G_{xz} (GPa)	G_{yz} (GPa)
R.R.L.	4.52	4.52	4.52	0.354	0.354	0.354	1.669	1.669	1.669
C.S.M.	9.14	9.14	5.484	0.328	0.197	0.328	3.44	1.371	1.371

Table 1: Material properties of the constituent materials.

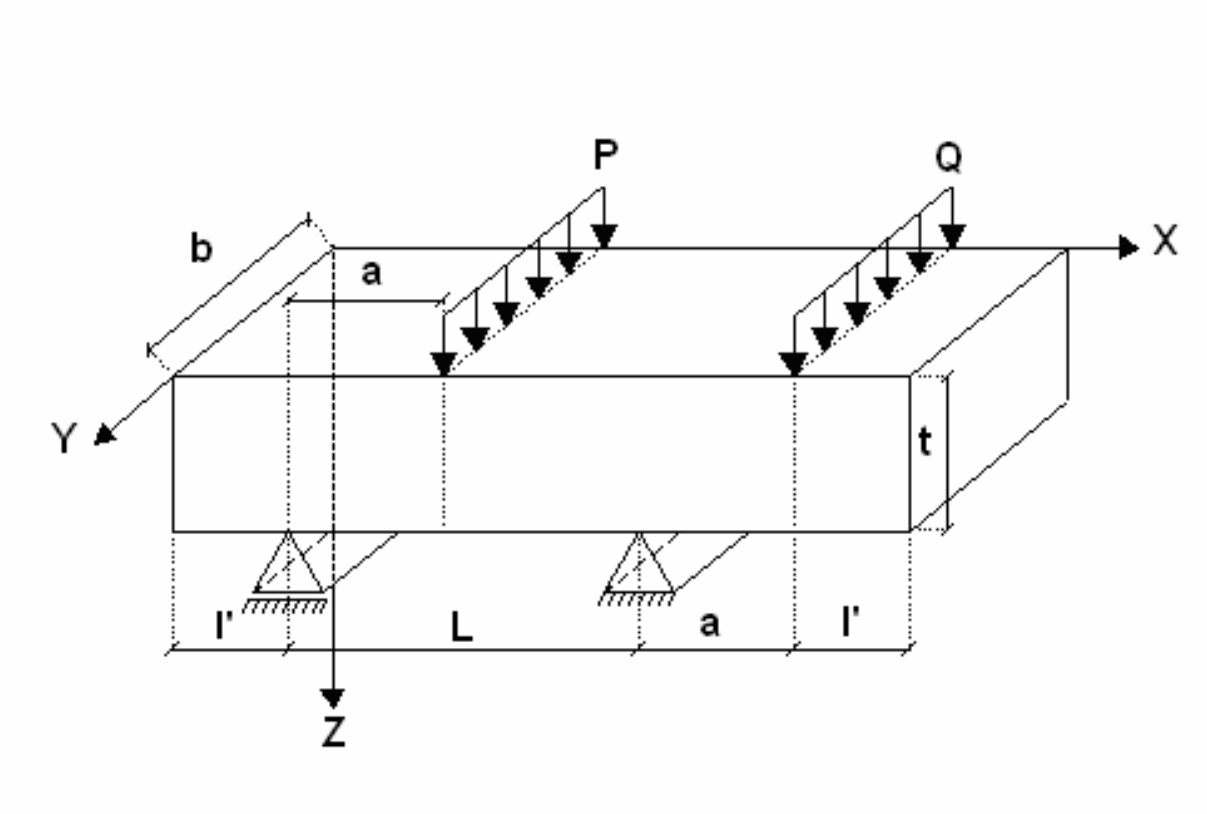

Figure 1(a): A composite beam in asymmetric four point bending

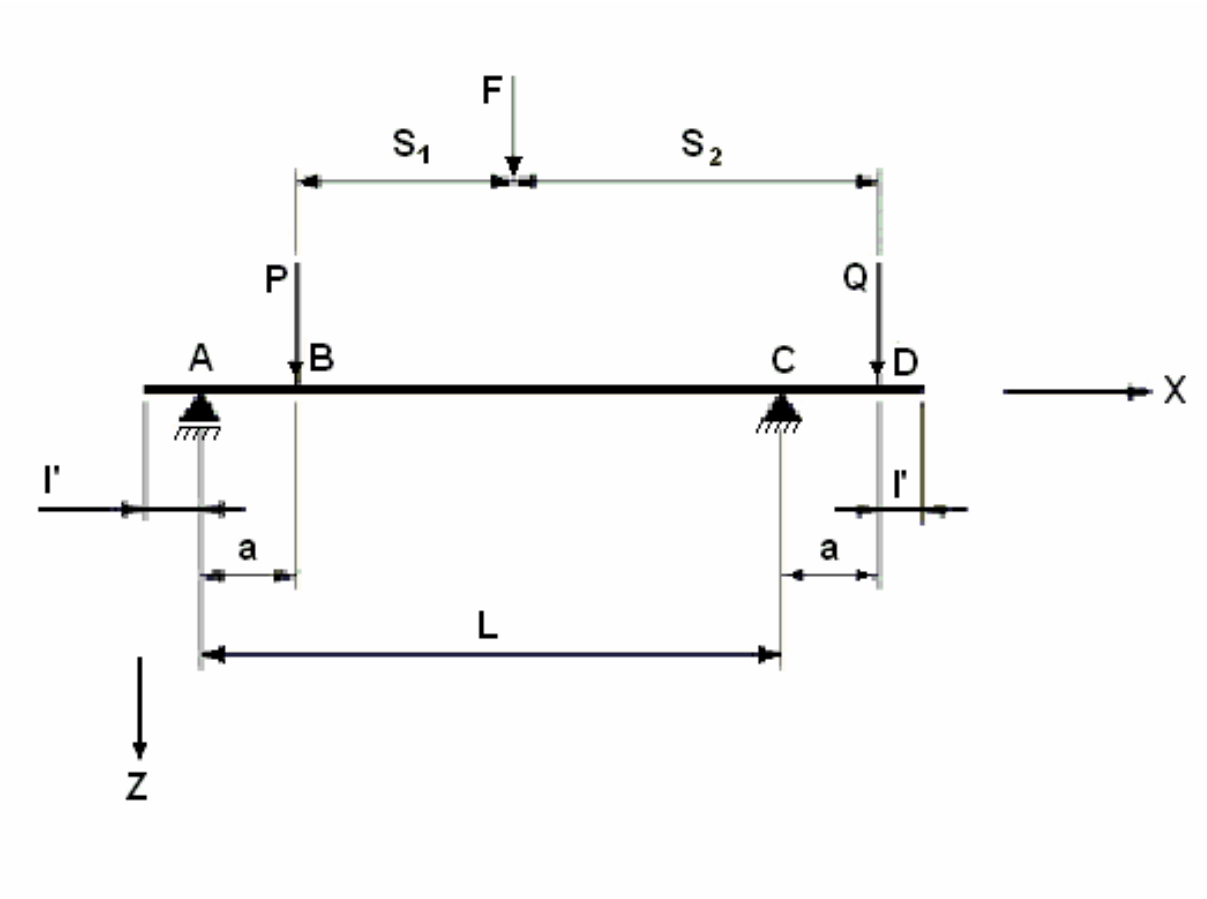

Figure 1(b): The laminates in asymmetric four point bending

In the recent literature several research works which confront the bending behavior of off-axis composites can be found. In [11] the longitudinal off-axis bending compliances of composites using four-point bending tests was examined whereas in [12, 13] analytical, numerical and experimental results have been developed in order to study the displacements field for any fiber orientation. On the other hand the nonlinear analysis of off-axis pultruded composite beams has been performed in [14] and the behavior of woven fabric composites in off-axis end-loaded bending using the theory of plastica in [15].

The main aim of this paper is to continue to shed some more light into the performances of thick composite beams under asymmetric off-axis four-point bending and to study the inter-laminar shear failure by investigating the asymmetric GRP laminates. For this reason composite specimens having Resin Rich Layers (RRL) thus forming asymmetric constructions have been considered (Laminate T3) as a continuation of a previous work carried out previously on symmetric laminates [16] made only from Chopped Strand Mat material (Laminate T1) (Fig. 2). The materials properties used in the analysis are given in Table 1.

According to a series of experiments in asymmetric four-point bending which had been performed on these laminates shear failure or flexural failure depending on the parameters introduced has been observed.

In the sequel, a three dimensional linear Finite Element Analysis (FEA) is carried out in the undamaged composite beams in order to, on the one hand, correlate with experimental results and, on the other hand, to obtain the stress distribution versus the vertical axis of the beam at the supports and at the loading points where usually there is an abrupt variation due

to the indentation existing because of the noses. Finally from the FEA, possible crack initiation positions have been identified and compared with those from the experimental work.

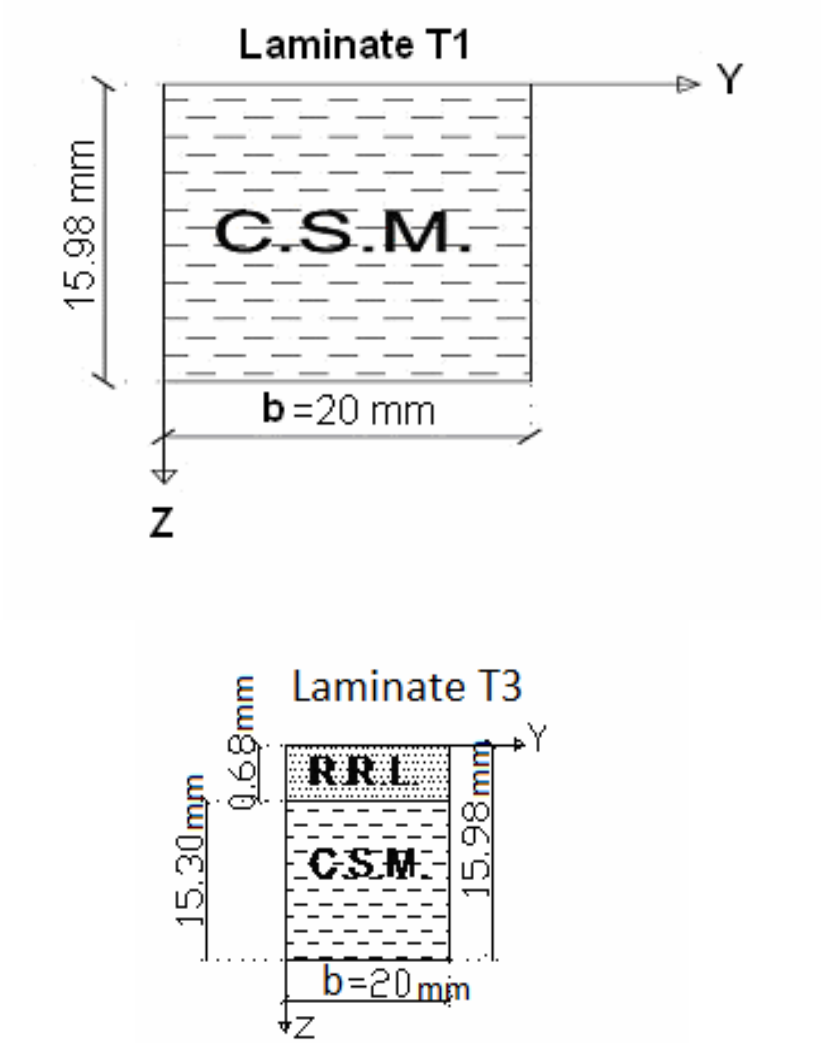

Figure 2: The laminates T_1 and T_3 used in asymmetric four point bending

2 ANALYSIS OF THE OFF-AXIS BENDING PROBLEM

Let us consider the asymmetric four point loading shown in Figures 1(a) and 1(b) where the applied load F is divided into unequal parts P and Q, which are equal to the supports forces at points A and C respectively.

From equilibrium and geometrical considerations, it is easily obtained

$$P=\frac{FS_2}{1+\lambda},\quad Q=\frac{FS_1}{L}, \tag{1}$$

$$\frac{P}{Q}=\frac{S_2}{S_1}=\lambda,\quad Q=\frac{F}{1+\lambda},\quad \mathrm{a}=\frac{\lambda-1}{\lambda+1}L \tag{2}$$

In the above relationships L is the distance between supports (span length), a is the distance between the support A (or C) and the loading point at B (or D) (Fig. 1(b)) and λ is the loading factor.

The stresses at any point in the beam can be calculated to a first approximation by using the mechanics of materials theory [6]. Thus the normal stress σ_{xx} has its maximum value at points B and C (Fig. 1(b)) as:

$$\sigma_{xx} = \frac{6F(\lambda-1)L}{(1+\lambda)^2 bt^2}, \tag{3}$$

where b and t designate the width and thickness of the beam respectively as it can be seen in Fig.1(a).

Similarly the maximum shear stress at the part (BC) of the beam is:

$$\sigma_{xz} = \frac{3(1-\lambda)F}{2(1+\lambda)bt} \tag{4}$$

Dividing the last two equations, it is obtained:

$$\frac{\sigma_{xx}}{\sigma_{xz}} = \frac{4L}{(1+\lambda)t} = C, \tag{5}$$

where C denotes the ratio of maximum normal stress to maximum shear stress at failure.

Thus it can be observed that in the off – axis four point test method in addition to span length / thickness (L/t) ratio which is the main parameter in the three point bending and symmetric four point bending tests, the loading factor λ (= P/Q) defining the ratio of the forces at the supports becomes an important parameter which characterizes the type of failure i.e. shear failure at the neutral axis near the middle plane or tensile (or compressive) flexural failure at the upper or lower part of the laminate beam.

According to the Bernoulli-Euler theory, the elastic deflection arising from a flexural-stress at point B (Fig. 1) in a rectangular beam is [6]:

$$\delta_F = \frac{8\lambda(\lambda-1)^2 FL^3}{E(\lambda+1)^5 bt^3} \tag{6}$$

The elastic shear deflection at the same point is:

$$\delta_S = \frac{12\lambda(\lambda-1)FL}{5G(\lambda+1)^3 bt} \tag{7}$$

The ratio of shear modulus to elastic modulus $\left(\frac{G}{E}\right)$ is much lower for composites than for the metals and hence shear deformation is more significant in composites.

The total deflection δ_t is the sum of the bending and shear components, that is

$$\delta_t = \delta_F + \delta_S = \frac{4\lambda(\lambda-1)FL}{(\lambda-1)^3 bt}\left\{\frac{2(\lambda-1)}{E(\lambda+1)^2}\left(\frac{L}{t}\right)^2 + \frac{3}{5G}\right\} \tag{8}$$

and the ratio of the two deflections is

$$\frac{\delta_S}{\delta_F} = \frac{3}{10}\left(\frac{E}{G}\right)\left(\frac{t}{L}\right)^2 \frac{(\lambda+1)^2}{\lambda-1} \tag{9}$$

It can be seen that $\frac{\delta_S}{\delta_F}$ depends not only on the ratio of the two modules and the span length-thickness ratio, which characterize symmetric three-point and four-point bending tests, but also on the loading factor λ

The apparent flexural modulus E_α can be found by assuming that the total deflection δ_t is due to flexure only, and is given by:

$$E_\alpha = \frac{8\lambda(\lambda-1)^2 FL^3}{(\lambda+1)^5 bt^3 \delta_F\left(1+\frac{\delta_S}{\delta_F}\right)} \tag{10}$$

For the apparent flexural modulus to be as nearly equal to the true flexural modulus as possible, the shear deflection must be compared to the flexural deflection that is

$$\frac{\delta_S}{\delta_F} \ll 1$$

3 EFFECTS OF SURFACE RESIN-RICH LAYER.

The existence of non-uniformity in a laminate generally influences the stresses and the moduli. In particular, a resin-rich layer on either or both of the surfaces can significantly affect the flexural modulus.

Since the tensile modulus of the fibre is much larger than that of the resin, the direct contribution of the latter to the ability of a fibre-reinforced laminate to resist flexural deformation is usually small, and can be neglected as a first approximation. Therefore, resin layers on the outer surface of a laminate have little influence on the deflection of a laterally loaded beam. However, surface resin-rich layers contribute to the laminate thickness which is used in computing moduli, and can therefore; have a significant effect on the computed flexural modulus.

If a laminate composite of total thickness *t* has resin-rich layers (RRL) on either or both surfaces of combined thickness, t_{RRL} , then the thickness of the part of the composite containing reinforcing fibres is

$$t_0 = t - t_{RRL} \tag{11}$$

At first, it is easily observed that the existence of surface RRL can affect determination of the fibre content, υ_f , of a composite as it is obtained from burn-off tests. Allowance can be made for this using the following expression (See Appendix)

$$\upsilon_{fc} = \frac{1}{1-\frac{t_{RRL}}{t}}\upsilon_f \tag{12}$$

From Eq. (3) by taking into account the RRL it can be obtained that:

$$\sigma_{xx} = \frac{6F(\lambda-1)L}{(\lambda+1)^2 bt_0^2},\ \sigma'_{xx} = \frac{6F(\lambda-1)L}{(\lambda+1)^2 bt^2},$$

where the bending normal stress of the laminate of thickness t be σ'_{xx} and for the laminate without resin rich-layer be σ_{xx}.

Thus, by dividing

$$\frac{\sigma'_{xx}}{\sigma_{xx}} = \frac{t_0^2}{t^2} = \left(\frac{t - t_{RRL}}{t}\right)^2 = \left(1 - \frac{t_{RRL}}{t}\right)^2 \simeq 1 - 2\frac{t_{RRL}}{t} \tag{13}$$

Similarly for the shear stress from Eq. (4) by taking into account the RRL can be obtained that :

$$\sigma_{xz} = \frac{3}{2}\frac{(1-\lambda)F}{(1+\lambda)bt_0},\ \sigma'_{xz} = \frac{3}{2}\frac{(1-\lambda)F}{(1+\lambda)bt}$$

where σ'_{xz} and σ_{xz} denote the shear stress of the laminate of thickness t and the laminate without RRL respectively. Again by dividing

$$\frac{\sigma'_{xz}}{\sigma_{xz}} = \frac{t_0}{t} = \frac{t - t_{RRL}}{t} = 1 - \frac{t_{RRL}}{t} \tag{14}$$

Eqs. (13) and (14) show that laminate stresses are sensitive to t_{RRL} which is highly variable in a hand lay-up composite and suggests that caution should be exercised in interpreting test results.

Let the apparent flexural modulus of the laminate of thickness t be E'_α.and for the laminate without resin-rich layers be E_α From Eq. (10) if the laminate deflections under load F are equated,

$$E'_\alpha = E_\alpha \left(\frac{t_0}{t}\right)^3 \tag{15}$$

Using Eq. (11) this can be written in terms of total thickness and resin-rich layer thickness :

$$E'_\alpha = E_\alpha \left(1 - \frac{t_{RRL}}{t}\right)^3 \simeq E_\alpha \left(1 - \frac{3t_{RRL}}{t}\right) \tag{16}$$

It can be observed that the resin-rich layer has a more significant effect on the apparent flexural modulus than on the stresses when Eq. (16) is compared with Eqs. (13), (14). This effect is double and triple with respect to the other two cases for the stresses.

4 EXPERIMENTAL WORK AND RESULTS

The materials used during the off-axis bending experiments were flat GRP laminates produced by Resinform Ltd using Atlac 382-OSA polyester resin modified by Bisphenol and reinforced with powder bound glass fiber-Chopped Strand Mat (CSM).

The lamination procedure gives usually rise to Resin – Rich surface Layers (RRL) which in practice is provided for corrosion resistance. In order to study the effect of a RRL and also to create an asymmetric laminate, the uneven (rough) side of the laminate was machined, thus avoiding the variations in the thickness of the specimens, factor which plays important role during bending.

The fibre content fraction M_f was determined from burn – off tests according to British Standards (BS) 2782. The result was $M_f = 0.33 \pm 0.01$. For each panel specimens were cut from each of the two perpendicular directions using a band-saw. The edges of the specimens were machined in a milling machine to the shape of a prismatic specimen having total nominal length of 10mm and nominal width of 11mm according to the above BS.

Before testing, the width and thickness of each specimen were measured with a micrometer at three points inside the specimen length. From these measurements, mean values of thickness and width were calculated for each specimen.

The experimental test apparatus consisted of an adjustable anvil which was mounted on a circular base that fits onto a compressive load cell on a Instron Universal testing machine of 100kN capacity. The radius of a loading nose and support nose is 5mm according to BS 2782. Before the tests the load cell should be calibrated. By employing strain-gauges and Linear Variable Displacement Transducers (LVDT), the stress strain and load-deflection curves can be plotted to determine material properties. A Peckel automatic data logger with an Anadix printer was used to record the strain and deflections. The cross-head was 0.5mm/min.The specimen shape and dimensions (Fig. 2) are as follows: $L = 56\text{mm}$, $a = 18.7\text{mm}$, $l' = 10\text{mm}$ and a loading factor $\lambda\left(= P/Q = 2\right)$. The CSM layers had a thickness of 15.30mm whereas the RRL had a thickness of 0.68mm, thus obtaining a total thickness of $t = 15.98\,\text{mm}$.

Four rectangular specimens were used for each laminate with a nominal thickness of 16mm and a width of 20mm after machining. During the tests, photos of some specimens had been taken of to record the crack formation process and the type of failure (flexural, shear or mix). From the experimental investigation the beams usually fail in shear at the (BC) region of the beam (Fig. 1a, 1b), namely between the load P and the right support C where cracking appeared at the middle plane depending on L and λ values.

Consequently by varying L and λ (with constant laminate thickness) one can obtain the two types of failure. For shear failures the ratios of $\max \sigma_{xx}$ to $\max \sigma_{xz}$ at failure should be grouped below C (Eq. 5) and for flexural failures the ratios of $\max \sigma_{xx}$ at failure to $\max \sigma_{xz}$ should be grouped above C. However, in some cases, there is a transitional (mix) case where the mode of failure changes from specimen to specimen.

The following observations had been made from the experiments [6]. An increase in normal stress σ_{xx} with increasing L/t or decreasing λ is apparent. In addition, it had been observed that the shear strength depends upon L/t and λ even for shear failures. This effect, which can be related to the discrepancies observed during the calculations, could be due to local stress concentrations, especially at the loading noses or the supports which are ignored in the simple beam theory. Alternatively, it could be a combined stress effect. If the shear strength is enhanced by the presence of a transverse compressive stress, then an increase in shear strength at smaller L/t would be expected.

Also, the effects of indentation near the supports or loading noses where the stresses change in an abrupt manner can be the reason of the shift and the different variation mainly in the shear stress obtained also by the FEA near and far off the supports, as it is exposed later.

Finally as to the influence of the existence of a RRL in the material, the fibre weight fraction M_f was determined from burn-off tests according to BS 2782 as $M_f = 0.330 \pm 0.01$. The corresponding volume fraction from Eq. (A1) is $\upsilon_f = 0.190 \pm 0.01$. From Equation (12) by excluding the RRL this value becomes $\upsilon_{fc} = 0.197$, whereas the experimental value from burn-off tests for the same materials without RRL is $\upsilon_{fc} = 0.200 \pm 0.01$.

Also from Equations (13)-(15) excluding the RRL of thickness $t_{RRL} = 0.68mm$ we obtain for the laminate of thickness $t \cong 16mm$

$\sigma'_{xx} = 0.915\sigma_{xx}, \sigma'_{xz} = 0.958\sigma_{xz}$ and $E'_a = 0.875E_a$ respectively.

The results show the influence of RRL on these properties of the laminate.

5 THREE DIMENSIONAL FINITE ELEMENT ANALYSES

A main goal of this paper is to investigate through the Finite Elements Analysis (FEA) some points which are difficult to clarify by experiments and/or analytical solutions and also if it is possible to make a correlation among them. Indeed, it is not easy to find out what occurs near the loading points and near the supports during a bending test where there is an abrupt change in some magnitudes such as bending moments which influence the stresses.

The fact that the test method used is an asymmetric off-axis bending, in our opinion, makes the investigation more difficult when compared to a symmetric four points or three point bending test. Therefore, a precious numerical method such as FE can contribute for understanding many issues and points and thus can act as a complementary useful tool to detect possible irregularities. Consequently, we consider that both methods experiments and FE constitute a totality and complete each other.

The uncracked laminates T3 are studied numerically in asymmetric off-axis four point bending by using the general purpose finite element program ANSYS [17]. In the three-dimensional analysis, the entire beam is modeled and the domain is filled with 8-node solid brick elements (SOLID 45). In order to verify our numerical results three finite elements meshes have been used with different mesh refinement with 18, 36 and 54 elements in the thickness direction at the part (BC) (Fig.1) of the beam where the maximum shear stresses are appeared. The results for the 36 and 40 elements in the thickness direction are almost similar.

5.1 Analysis of the T3 Specimen

In the three dimensional finite element mesh considered, the width of the beam is discretized with 20 elements, the thickness of the beam with 37 elements, and the length of the beam at the parts (AB) and (CD) (Fig. 1) with 30 elements. In the thickness direction 6 elements are considered in the upper RRL and 31 elements in the lower CSM. The loads at failure are taken P=14800N, and Q=7400N from the experimental investigation [6].

The deflection obtained by the finite element method at point B (Fig. 1(b)), are taken at the same surface points where the deflection are measured in the experiments and an average value of them $\delta\left[=\left(\delta L_1 + \delta L_2\right)/2\right]$ is given in Table 2. The maximum deflection appeared in the middle section at the end of the beam (x= 94.7mm, y= 10mm, z= 15.98mm)

From the stress analysis of the simple supported composite beam of laminate T3 in asymmetric bending, the maximum normal stresses appeared (Fig. 3) at the point B where the load P is applied and at the support C (Fig.1(b)), where the moments and the shear forces take their maximum values. The maximum shear stresses appeared at the parts (BC), (AB) and (CD) of the beam where the shear forces take their maximum values.

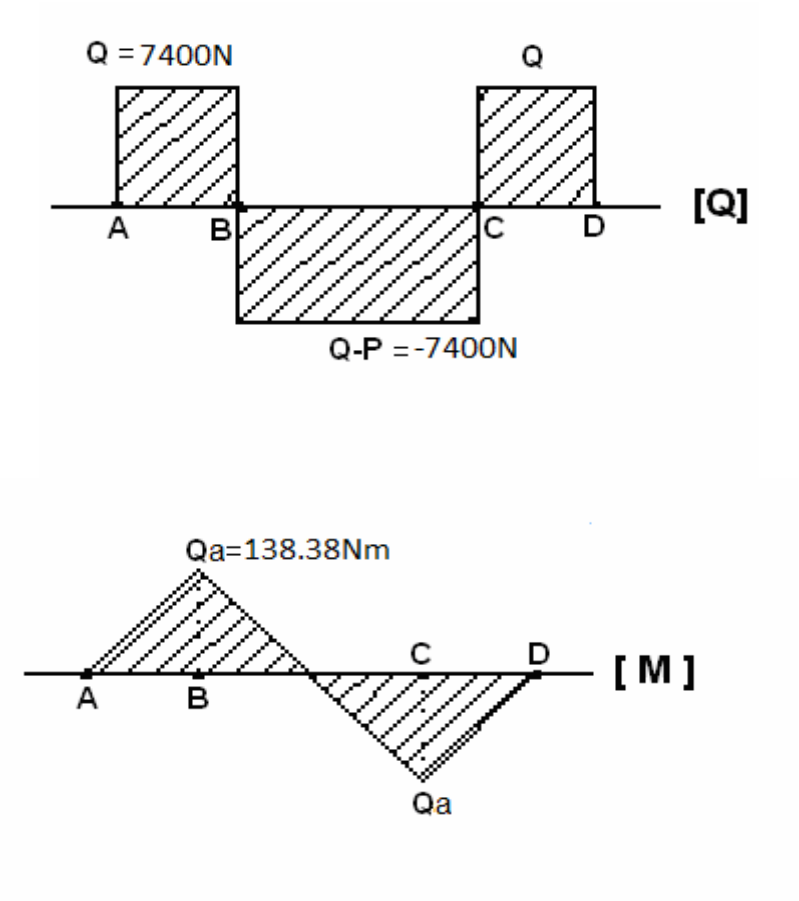

Figure 3: The diagrams of shear forces Q and bending moments M of the laminate T3 in asymmetric bending

From the three dimensional finite element analyses the maximum reasonable normal and shear stresses are also given (Table 3). The maximum σ_{xx} and σ_{xz} stresses are determined at a middle longitudinal cross section of the beam. The max σ_{xx} and σ_{xz} are found at a distance about 2.5 mm to the left of the point B (Fig. 1) where the load P is applied inside the CSM material and close to the interface ($z \simeq 1.1$ mm) between the CSM and RRL materials of the T3 specimen. High σ_{xx} and σ_{xz} stresses are also observed near the right support C, and high σ_{xz} near the middle of the part (BC) of the beam.

Deflection	Max(x= 94.7mm)	B(x=28.7mm)
δ	1.545mm	1.179mm

Table 2: Deflections from the finite element analysis for laminate T3.

Maximum Stresses	Close to B (x ≃ 26.12 mm)	Close to C (x ≃ 76 mm)	Between B and C (x ≃ 47.4 mm)
$\max \sigma_{xx}$	175.51MPa	140.695MPa	2.087
$\max \sigma_{xz}$	43.475MPa	36.358MPa	33.301

Table 3: The $\max \sigma_{xx}$ and $\max \sigma_{xz}$ stresses from the finite element analysis for laminate T3.

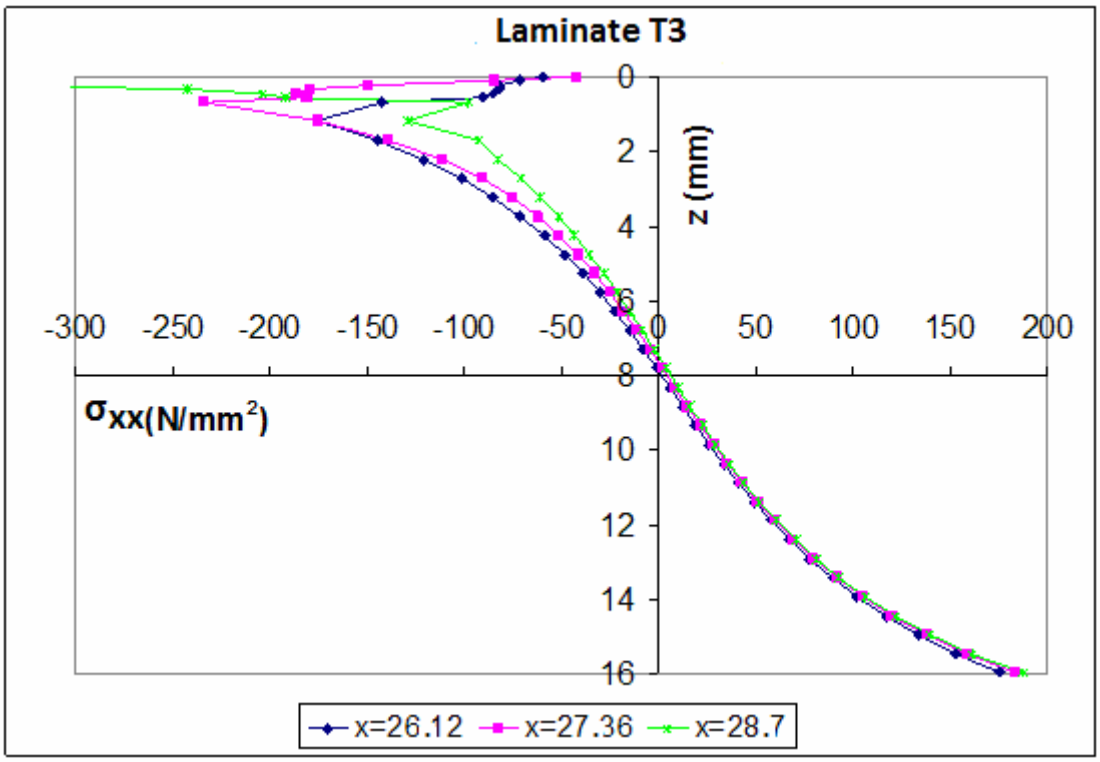

Figure 4: σ_{xx} -stress distributions through the beam thickness of laminate T3 close to point B where the load is applied.

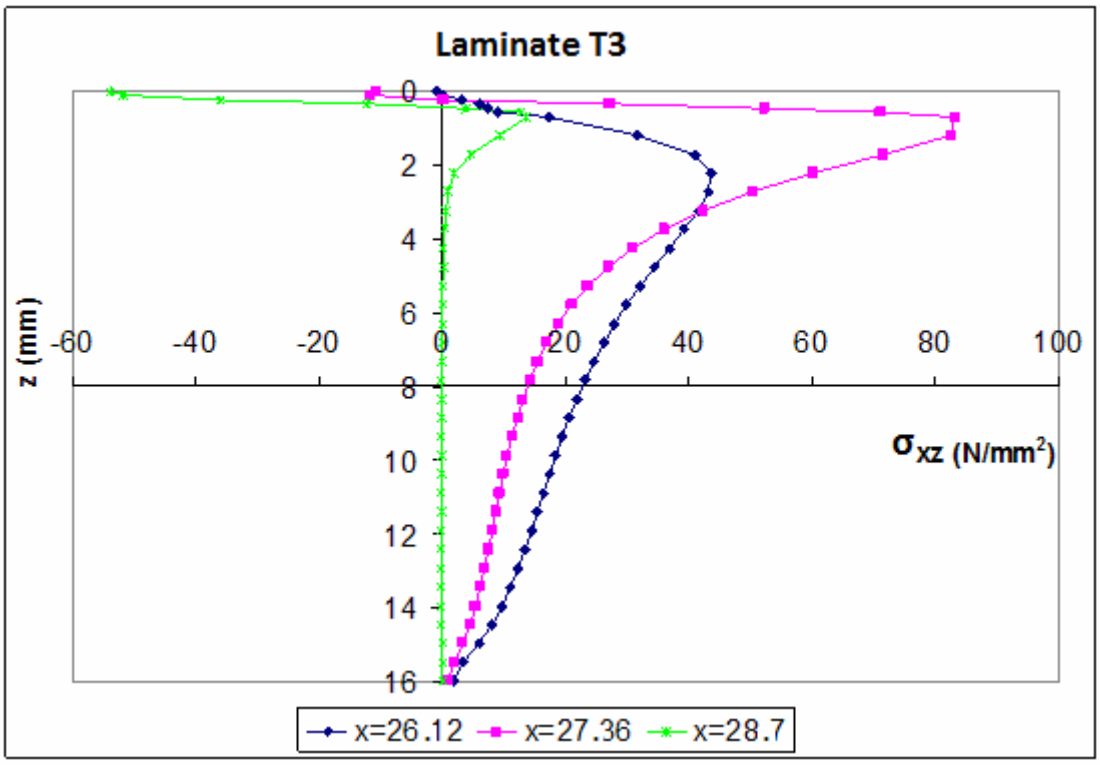

Figure 5: σ_{xz} -stress distributions through the beam thickness of laminate T3 close to the point B where force P is applied.

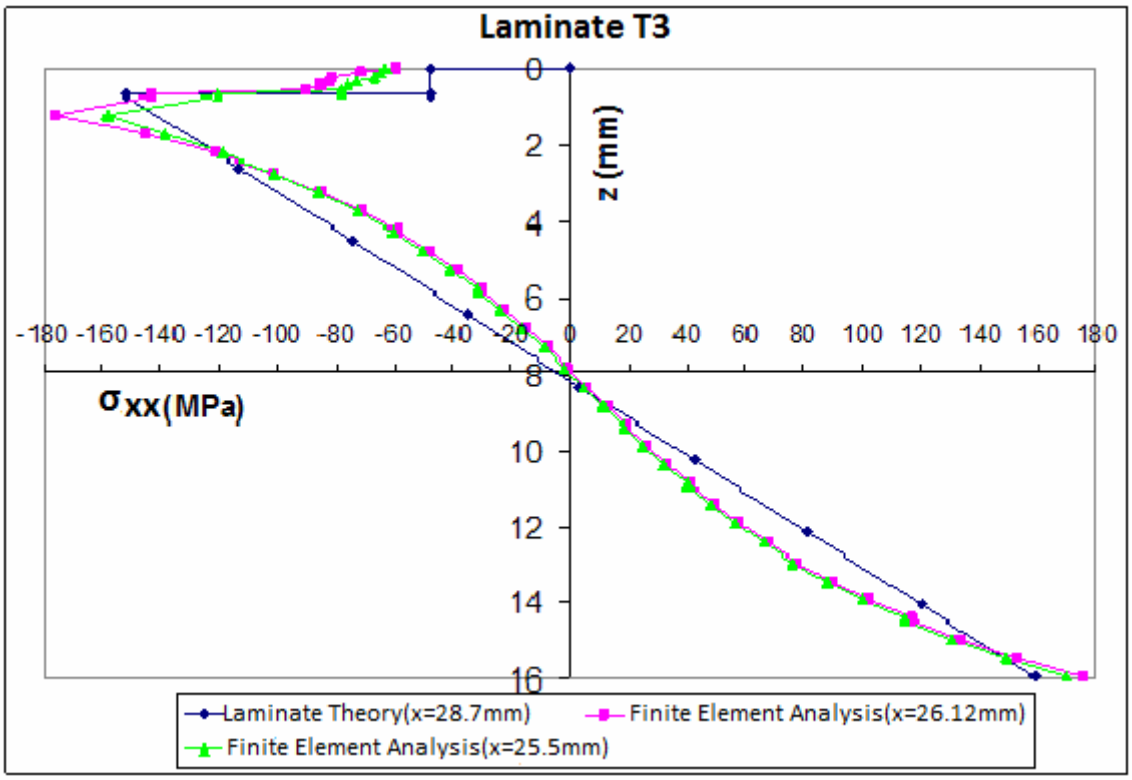

Figure 6: σ_{xx} -stress distributions through the beam thickness of laminate T3.

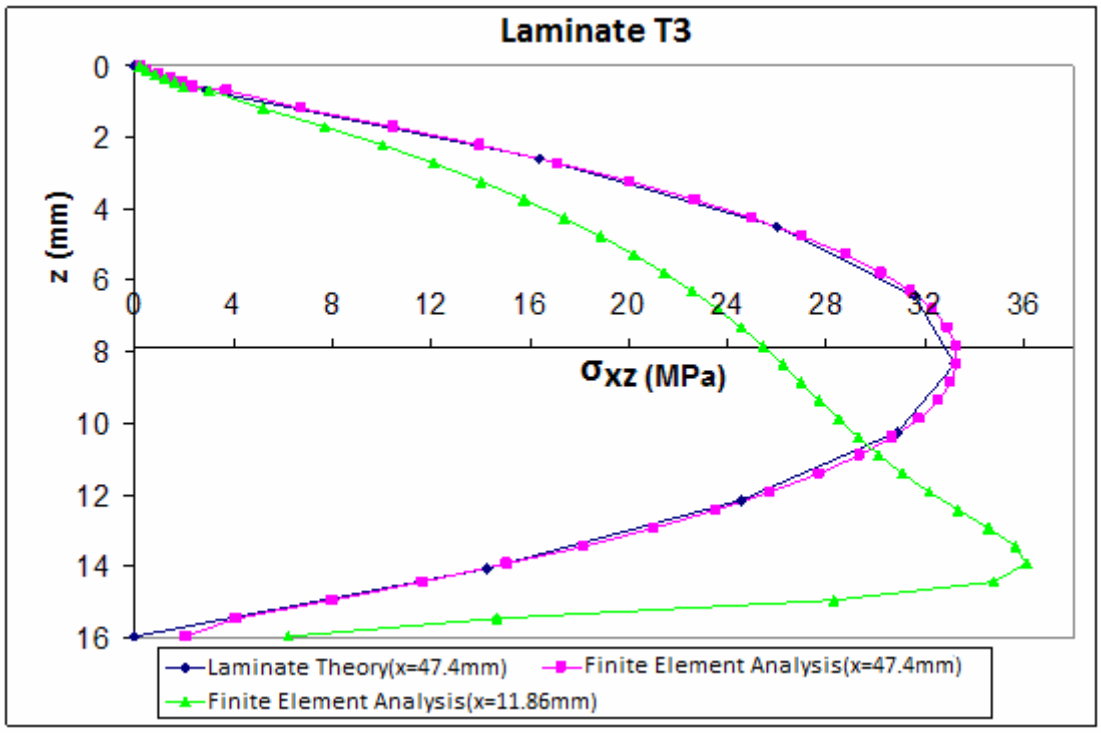

Figure 7: σ_{xz} -stress distributions through the beam thickness of laminate T3.

T3 Point B	(i) Laminate theory	(ii) FEA x= 26.12mm	Percentage Difference (ii)- (i) (%)	(iii) FEA x= 25.5mm	Percentage Difference (iii)- (i) (%)	
max σ_{xx} (MPa)	151.95	175.51	13.4	158.07	3.9	Interface(z=0.68)
max σ_{xx} (MPa)	158.94	175.54	9.45	169.88	6.4	Lower tensile fiber (z=15.98)

Table 4: Percentage differences between the laminate theory and FE results for $\max \sigma_{xx}$ of laminate T3 close to the point B where the force P is applied.

T3 Point C	(i) Laminate theory	(ii) FEA x= 47.4mm	Percentage Difference (ii)- (i) (%)	(iii) FEA x= 11.86mm	Percentage Difference (iii)- (i) (%)
max σ_{xz} (MPa)	33.224	33.301	0.23	36.110	8.7

Table 5: Percentage differences between the laminate theory and FE results for $\max \sigma_{xz}$ stresses of laminate T3.

In Figure 4 the variation of normal σ_{xx} stress distributions obtained from FEM calculations are given near the point B (x=28.7mm) and at different distances from it, where the maximum

reasonable σ_{xx} is obtained. It is observed that at the point B the σ_{xx}-distribution tend to very high values as it was expected from linear theory of elasticity. The σ_{xx}-distributions as we move away from the support approach the linear variation. In addition the σ_{xz}-distributions close to the point *B* and at different distances from it are given in Figure 5. It is observed that the σ_{xz}-distributions as we move away from the singular point B tend to become parabolic as it was expected from laminate theory. However by taking into consideration Equation (5), the ratios of the maximum normal to the maximum shear stresses from the FEA (Table 3) at the parts of the beam where the maximum stresses appeared, were always lower than the values of C (=4.673) for laminate T3. Hence it is also verified from the finite element analysis that the laminate T3 fails in shear. Furthermore from the finite element analyses and the maximum σ_{xx}, σ_{xz} stresses (Table 3) developed in the beam it is verified that the RRL material has already failed in flexure. This happens because the max σ_{xx} stresses overpass the stress failure in flexure of the RRL material about 47.5 MPa determined experimentally [6].

In Figure 6 he distribution of maximum normal stress, σ_{xx} *vs* the laminate thickness as obtained from laminate theory in Equation (3) and also from finite elements method (FEM) is illustrated. It can be observed that the stress variation according to laminate theory shows a linear variation, as expected, similar to that of a simple beam considering that the RRL layer has already failed. Nearly the same variation is also obtained from FEM calculations far off the supports (x=26.12mm, 25.5mm). The stress distribution is not completely linear. It is like a small curve. It reminds the normal stress distribution in curved beams where σ_{xx} - has a hyperbolic distribution. In addition the percentage differences between the laminate theory and the FEA close to the point B where the maximum σ_{xx} stresses appear, at the interface between the RRL and CSM materials and at the lower part of the laminate beam are presented in Table 4. On the other hand in Figure 7 the distribution of maximum shear stress, σ_{xz} *vs* the laminate thickness as obtained from laminate theory in Equation (4), and from FEA is illustrated. It can be observed that the stress variation according to laminate theory shows a parabolic variation as expected, similar to that of a simple beam. Nearly the same variation is also obtained from FEM calculations far off the supports ($x = 47.4mm$). However, the variation of shear stress obtained from FEA is very different near the support A (Fig. 1(b)) i.e. at $x = 11.86mm$. The parabolic variation with a maximum at the neutral axis becomes a curve with a different shape the maximum of which shifts to the lower part of the laminate beam as in the case of failures due to normal stress (tensile or compressive) where the specimen fails either at its lower part or at the upper part, which it does not occur in our case where from the experiments a shear failure at the neutral axis was observed. In addition the percentage differences between the laminate theory and the FEA results for the maximum σ_{xz} stresses in the middle of the part (BC) (Fig. 1(b)) and close to the support A, are presented in Table 5.

6. CONCLUSIONS

The study of asymmetric glass reinforced plastic beams in asymmetric off-axis four point bending was examined experimentally and numerically.

At first an experimental investigation was carried out where specimens were tested to failure. From the experimental verification and from a wide range of tested specimens it was shown that the main observation is that they fail in shear at the part of the beam between the area where the load was applied and the right support of the beam (Fig. 1(b)). From the experiments was also observed that it was difficult to find out what occurs near the loading

points and near the supports during a bending test where there is an abrupt change in bending moment which influences the stresses fact that, in our opinion, can be thoroughly investigated by FE Method.

A linear three dimensional finite element analysis was performed. It was used a linear FE analysis because the behavior of the corresponding composite beams for laminates T1 (Fig.2) [16] from the experiments, was up to the failure linear. Considering the stress picture for the failure loads obtained from the experiments, the main problem from the numerical investigation was also in shear into the same part of the beam where shear failure was observed from the experiments, between the right support of the beam and the point B where the load P was applied. This was also verified from Equation (5), because the ratios of the resulted maximum stresses from the finite element analysis were always lower than $C(=4L/(1+\lambda)t)$. Thus, initial crack formation may occur in the middle plane of the T3 material and inside the CSM material.

From the proposed analysis results that the classical laminate theory in the case of asymmetric glass reinforced plastic beams in asymmetric off-axis four points bending could not accurately predict the failure of composite beams. In addition the introduction of the external RRL material (T3 specimen) although influences in some extent the fibre content, the stresses and the elastic modulus as evaluated, does not affect substantially the interlaminar shear strength of GRP specimens because of the lower flexural strength of it comparing with the CSM material.

REFERENCES

[1] R. Kitching, J. N. Ashton, E. Sideridis, An interlaminar shear test for fibre reinforced plastics. *COMP 88 Symposium on Phase Interaction in Composite Materials*, The University of Patras, Greece, 1988.

[2] A. S. Clarke, A study of differences of strength properties and geometric variations of commercially produced straight GRP piping from three manufacturers. *MSc Dissertation*, University of Manchester, 1980.

[3] C. J. Kirk, Effect of geometric design parameters on the flexural behaviour of glass reinforced plastic pipe intersections. *PhD thesis*, University of Manchester, 1980.

[4] A. L. Tan, Strength and flexibility of glass reinforced plastic pipes and pipe bends. *PhD thesis*, University of Manchester, 1983.

[5] P. Myler, Glass reinforced plastic pipe bends under a variety of loads. *PhD thesis*, University of Manchester, 1985.

[6] E. Sideridis, J.N. Ashton, R. Kitching, Measurement of the interlaminar shear stress of glass-reinforced plastics of different construction using the off-axis four point bending test. *Composite Structures*, **18**, 139-161, 1991.

[7] L.A. Carlsson,. J.W. Gillespie Jr, R.B. Pipes, On the analysis and design of the End Notched Flexure (ENF) specimen for mode II testing. *Journal of Composite Materials*, **20**, 594-604, 1986.

[8] L.A. Carlsson, J.W. Gillespie, Interlaminar shear fracture of interleaved graphite/epoxy composites. *Composites Science and Technology*, 43, 55-69, 1992

[9] E.E. Theotokoglou, D. Hortis, L.A. Carlsson, H. Mahfuz, Numerical study of fractured sandwich composites under flexural loading. *Journal of Sandwich Structures and Materials*, **10**, 75-94, 2008.

[10] E. E. Theotokoglou, I. I. Tourlomousis, Crack kinking in sandwich structures under three point bending. *Theoretical and Applied Fracture Mechanics*, **53**, 158- 164, 2010.

[11] M. Grediac, Four–point bending tests on off-axis composites. *Composite Structures*, **24**, 89-98, 1993.

[12] F. Mujika, I. Mondragon, On the displacement field for unidirectional off-axis composites in 3-point flexure – Part 1: Analytical approach. *Journal of Composite Materials*, **37**, 1041-1066, 2003.

[13] F. Mujika, A. De Benito, I. Mondragon, On the displacement field for unidirectional off-axis composites in 3-point flexure – Part II: Numerical and experimental results. *Journal of Composite Materials*, **37**, 1191-1217, 2003.

[14] H. Killic, H.-A. Rami, Elastic-degrading analysis of pultraded composite structures. *Composite Structures*, **60**, 43-55, 2003.

[15] P. K. Majumdar, P. Fazzino, K. L. Reifsnider, Behavior of woven fabric composites in off-axis end-loaded bending. *International SAMPE Symposium and Exhibition (Proceedings).* Baltimore, MD, USA, Code 79037, Volume 54, May 18-21, 2009.

[16] E.E. Theotokoglou, E. Sideridis, Study of composite beams in asymmetric four-point bending. *Journal of Reinforced Plastics and Composites*, **30**, 1125-1137, 2011.

[17] ANSYS Engineering Analysis System, *User's Manual*, Swanson Analysis Systems, Inc., 2007.

APPENDIX

Determination of the volume fraction υ_f of fibres, given the weight fraction of the fibres.

The British Standards (BS), method of determining υ_f of fibres is to burn off the resin from a measured portion of the specimen. This gives the percentage weight of the glass fibres:

$$\upsilon_f = \frac{\dfrac{M_f}{\rho_f}}{\dfrac{M_f}{\rho_f}+\dfrac{M_m}{\rho_m}} = \frac{1}{1+\left(\dfrac{M_m}{M_f}\right)\left(\dfrac{\rho_f}{\rho_m}\right)} = \frac{1}{1+\left(\dfrac{\rho_f}{\rho_m}\right)\left(\dfrac{1}{M_f}-1\right)}, \qquad (A_1)$$

where

$\upsilon_f, \upsilon_f =$ volume fraction of fibres and matrix.

$M_f, M_m =$ weight fraction of fibres and matrix

$\rho_f, \rho_m =$ specific density of fibres and matrix.

However, to obtain the volume fraction of a composite excluding the Resin-Rich Layer (RRL):

$$\upsilon_{fc}=\frac{\upsilon_f}{\upsilon_f+\left(\upsilon_m-\upsilon_{RRL}\right)}=\frac{\upsilon_f}{\upsilon_f+\upsilon_m-\left(\frac{t_{RRL}}{t}\right)\left(\upsilon_f+\upsilon_m\right)}=\frac{1}{\left\{1+\frac{M_m}{M_f}\left(\frac{\rho_f}{\rho_m}\right)\right\}\left(1-\frac{t_{RRL}}{t}\right)}=$$
$$=\frac{1}{1+\left(\frac{\rho_f}{\rho_m}\right)\left(\frac{1}{M_f}-1\right)\left(1-\frac{t_{RRL}}{t}\right)}=\upsilon_f\frac{1}{\left(1-\frac{t_{RRL}}{t}\right)}, \tag{A$_2$}$$

where

$t_{RRL}=$ thickness of the RRL, $t=$ total thickness.